RSC Advances

PAPER

Cite this: *RSC Adv.*, 2024, **14**, 1854

Experimental and DFT insights into the adsorption mechanism of methylene blue by alkali-modified corn straw biochar†

Huali Yu, ‡[a] Yulu Zhang,‡[a] Lianfeng Wang,*[a] Ya Tuo,[b] Song Yan,[a] Junling Ma,[a] Xue Zhang,[a] Yu Shen,[a] Haiyan Guo[a] and Lei Han[a]

As an efficient and cost-effective adsorbent, biochar has been widely used in the adsorption and removal of dyes. In this study, a simple NaOH-modified biochar with the pyrolysis temperature of 300 °C ($NaCBC_{300}$) was synthesized, characterized, and investigated for the adsorption performances and mechanisms of methylene blue (MB). $NaCBC_{300}$ exhibited excellent MB adsorption performance with maximum removal efficiency and adsorption capacity of 99.98% and 290.71 mg g^{-1}, which were three and four times higher than biochar without modification, respectively. This might be attributed to the increased content of –OH and the formation of irregular flakes after NaOH modification. The Freundlich isotherm suggested multilayer adsorption between $NaCBC_{300}$ and MB. Spectroscopic characterizations demonstrated that multiple mechanisms including π–π interaction, H-bonding, and pore-filling were involved in the adsorption. According to density functional theory (DFT) calculations, electrostatic interaction between $NaCBC_{300}$ and MB was verified. The highest possibility of the attraction between $NaCBC_{300}$ and MB was between –COOH in $NaCBC_{300}$ and $R–N(CH_3)_2$ in MB. This work improved our understanding of the mechanism for MB adsorption by modified biochar and provided practical and theoretical guidance for adsorbent preparation with high adsorption ability for dyes.

Received 1st September 2023
Accepted 30th November 2023

DOI: 10.1039/d3ra05964b

rsc.li/rsc-advances

1. Introduction

Numerous dyes have been utilized in diverse applications such as textile, paper, printing, painting, and rubber industries.[1] Previous studies have estimated that about 7 Mt of dyes are produced globally each year.[1,2] The disposal of dyes in the environment contaminates water bodies, affects the water quality, and damages to human health. Diverse separation techniques, including biological (microbial biomass, algae degradation, and enzyme degradation, *etc.*), chemical (advanced oxidation process, Fenton and photochemical reactions, *etc.*), and physical (adsorption, membrane filtration, and reverse osmosis, *etc.*) treatments have been applied for the removal of dyes from aqueous solutions.[3–5] Among these treatments, the adsorption of dyes has been considered one of the most commonly used methods owing to its simplicity and effectiveness.

Azo dyes have been the most widely used synthetic dyes in the printing and dyeing processes, which possess nonbiodegradable, toxic, and even carcinogenic properties.[6] Previous studies have demonstrated that azo dyes could be adsorbed by carbonaceous materials,[7,8] such as activated carbon,[9] graphene,[10] and carbon nanotubes.[11] The carbonaceous materials with high pore volume, wide distribution of pore size, and abundant functional groups would be conducive to the adsorption of azo dyes.[12] Recently, biochar has been considered a viable alternative owing to its low cost and wide range of sustainable feedstocks.[13] Biochar was obtained from biomass *via* thermal treatments under anoxic or anaerobic conditions,[14] and has been proposed as one of the most promising adsorbents for removing organic contaminants (*e.g.*, pharmaceuticals, pesticides, phenols, polynuclear aromatics).[15–18] However, the detailed interactions (*e.g.*, electrostatic interaction, π–π interaction, H-bonding) between biochar and the adsorbed dyes required further investigations.[19,20]

Compared to pristine biochar, modified biochar has been demonstrated to perform higher efficiency in dyes adsorption, and the modification methods such as physical modification (*e.g.*, steam, heat, and ball mill) and chemical modification (*e.g.*, alkali and acid) were commonly applied.[14,21,22] In comparison with physical modification, it has been suggested that chemical modification was cheaper, less time-consuming, and could produce more characteristic surface functional groups for

[a]*School of Environmental & Chemical Engineering, Dalian Jiaotong University, Dalian 116021, China. E-mail: wanglfdl@aliyun.com; Fax: +86-411-84107585; Tel: +86-411-84107585*

[b]*Environmental Development Center of the Ministry of Ecology and Environment, Beijing 100006, China*

† Electronic supplementary information (ESI) available. See DOI: https://doi.org/10.1039/d3ra05964b

‡ Huali Yu and Yulu Zhang contributed equally to this paper.

adsorption.[23,24] Previous researches have demonstrated that biochar modified by methanol, humic acid, and chitosan could considerably enhance its ability to adsorb contaminants.[25,26] However, the practical application of organic compounds would be limited by their high cost and the volatile characteristic of some organic solvents.[25] Fan *et al.* revealed that compared with acid modification, alkali-modified bamboo biochar could significantly improve the adsorption capacity of chloramphenicol.[27] Nevertheless, the specific alkali modification parameters required further optimization, and the detailed interacting functional groups between biochar and dyes deserved further investigation.

In this study, corn straw was selected as a low-cost and renewable biomass raw material for the preparation of biochar. The reasons for selecting corn straw for biochar preparation were its high yield in China and improper disposal *via* discarding or burning.[28] NaOH was utilized to modify biochar without high temperature and high pressure. The optimum modification parameters of alkali modification, the removal efficiency and adsorption capacity of methylene blue (MB) by the modified biochar were investigated. Additionally, the potential removal mechanisms including detailed interactions and primary functional groups between biochar and MB were investigated *via* both spectroscopic and density functional theory (DFT) computational analyses.[6,29,30] The findings of this work showed that alkali-modified biochar derived from agricultural residuals could be used for the treatment of dye pollution in wastewater, and realize resource utilization of agricultural waste.[31]

2. Materials and methods

2.1 Chemicals

MB, NaOH, HCl, and other chemicals were obtained from Damao Chemical Reagents (Tianjin, China). All the chemicals were of analytical grade. Deionized water was used throughout the experiments. In addition, corn straw was collected from Shuangtaigou Village (Dalian, China, 121° 36′E, 38° 97′N).

2.2 Preparation of biochars

The corn straw biomass was firstly cleaned and dried at 80 °C for 12 h, ground to powder, and passed through a 100-mesh sieve (0.15 mm). The prepared powder was subsequently pyrolyzed under nitrogen protection in a tube furnace at a rate of 5 °C min^{-1} for 4 h at 300, 400, 500, and 600 °C, respectively. After cooling down naturally, the pyrolytic samples were washed with HCl (0.1 M) and distilled water *via* centrifugation (5000 rpm, 10 min) until the pH of the suspension was achieved neutral, and oven-dried for 12 h at 60 °C (Fig. S1†). Finally, the biochar products were passed through a 100-mesh sieve and stored in the dark. The biochar samples pyrolyzed at 300, 400, 500, and 600 °C were hereafter termed as CBC_{300}, CBC_{400}, CBC_{500}, and CBC_{600} (CBCs), respectively.

2.3 Modification of biochars

The optimal preparation parameters were screened by a four-factor and four-level orthogonal experiment (Table S1†), including pyrolysis temperature (300, 400, 500, and 600 °C), solid–liquid ratio (1 : 10, 1 : 20, 1 : 30, and 1 : 40 (v/w)), NaOH concentration (0.5, 1, 1.5, and 2 M), and modification time (6, 12, 18, and 24 h). Sixteen samples prepared under different conditions were labeled as C1–C16 (NaCBCs, Fig. S1 and S2†). Based on the results of MB removal efficiency and range analyses R, the optimum pyrolysis temperature, NaOH concentration, solid–liquid ratio, and modification time could be identified as 300 °C, 1.5 M, 1 : 10 (v/w), and 18 h, respectively (Table S1†). The pyrolysis temperature was the only one of those four parameters to be statistically significant ($p < 0.05$) (Table S2†).

For the optimized alkali-modified biochar, CBC_{300} was immersed in 1.5 M NaOH at a solid–liquid ratio of 1 : 10 (v/w) for 1 h under stirring (220 rpm). The mixture was left to stand for 18 h. The resultant biochar was then rinsed with distilled water until the pH became neutral to remove the residual NaOH. The modified biochar sample was collected *via* pressure filtration and finally dried at 80 °C overnight. NaOH-modified CBC_{300} was hereafter named as $NaCBC_{300}$.

2.4 Batch experiments

All adsorption experiments were conducted in 250 mL conical flasks on oscillator (220 rpm) for 4 h at room temperature (25 °C ± 1 °C). After standing for 1 h, the supernatant was collected and centrifuged at 5000 rpm (10 min). The supernatant of the adsorption system was diluted with phosphate buffer and analyzed with UV-Vis spectrophotometer (UV-1800, AuCyBest, Shanghai) at 665 nm. To investigate the reusability of $NaCBC_{300}$, five successive cycles were conducted. After adsorption, the $NaCBC_{300}$ was washed with deionized water, dried for 24 h, and reused for the next cycle. All the adsorption experiments were performed in triplicate.

To investigate the adsorption ability of biochar samples, the removal efficiency R_e (%) and adsorption capacity q_e (mg g^{-1}) were calculated according to eqn (1) and (2):

$$R_e = \frac{(C_0 - C_e)}{C_0} \times 100\% \quad (1)$$

$$q_e = \frac{(C_0 - C_e)}{m} \times V \quad (2)$$

where C_0 and C_e (mg L^{-1}) represented the original and final concentration of MB; V (L) indicated the solution volume; and m (g) was the dosage of the adsorbent.

The Langmuir isotherm revealed the monolayer adsorption with specific homogenous sites within the adsorbent.[32] The non-linear form of the Langmuir isotherm could be described as (eqn (3)):

$$Q_e = \frac{Q_m K_L C_e}{1 + K_L C_e} \quad (3)$$

where C_e (mg L^{-1}) represented the equilibrium adsorption concentration, Q_e (mg g^{-1}) was the adsorption capacity at equilibrium, Q_m (mg g^{-1}) indicated the monolayer capacity, and K_L (L mg^{-1}) was the Langmuir constant.

Additionally, the Freundlich model was also applied to explain multilayer adsorption on the adsorbent surface,[33] which could be expressed as follows (eqn (4)):

$$Q_e = K_F C_e^{1/n} \quad (4)$$

K_F (mg^{1-n} L^{-n} g^{-1}) and n were constants of Freundlich, which respectively represent the adsorption capacity and the adsorption intensity.

2.5 Characterization methods

The surface morphology of the biochar samples was observed by scanning electron microscopy (SEM, SUPRA 55 SAPPHIRE, Carl Zeiss, German). The N_2 adsorption–desorption isotherms and pore distribution of the biochars were measured by automatic surface area and pore analyzer (NOVA-4000, Quantachrome, USA) at 77 K. The specific surface area (SSA) of the biochars was determined using the Brunauer–Emmett–Teller equation. X-ray diffraction (XRD, EMPYREAN, PANalytical, Netherlands) and Fourier transform infrared spectroscopy (FTIR, TENSOR II, Bruker, USA) were used to identify the crystal structure and functional groups of biochars. X-ray photoelectron spectroscopy (XPS, Thermo SCIENTIFIC ESCALAB 250Xi, USA) was applied to determine the electronic and atomic structures of the surface and interface of biochars.

3. Results and discussion

3.1 Characterization of biochars

SEM observations showed that $NaCBC_{300}$ possessed more irregular flakes than CBC_{300} (Fig. 1a and b), which might facilitate the adsorption process by accelerating the transportation of the pollutants.[34] Cui *et al.* have revealed that bamboo-derived activated carbon aerogel activated by KOH could facilitate the formation of extra pores, which resulted in a rough surface and porous structure, and thus promoted the adsorption of contaminants by providing more active sites.[35] Pyrolysis temperature also affected biochars' surface morphology. With the increase of pyrolysis temperature from 400 to 600 °C, more cracks and breakages and less indication of raw biomass structures were observed (Fig. S3†), which might be attributed to the decomposition of macromolecular compounds.[36]

According to the IUPAC classification, the nitrogen adsorption isotherms were determined as type IV with a wide hysteresis loop for both CBC_{300} and $NaCBC_{300}$, which manifested that the porosity of biochars was mainly composed of micropores and mesopores (Fig. S4†).[33,37] The specific surface area (SSA) of $NaCBC_{300}$ (92.0 m^2 g^{-1}) was lower than that of CBC_{300} (101.2 m^2 g^{-1}), while the average pore size (AP) of $NaCBC_{300}$ (10.2 nm) was larger than that of CBC_{300} (8.6 nm) (Table S3†). Additionally, the TPV of $NaCBC_{300}$ (0.142 cm^3 g^{-1}) and CBC_{300} (0.157 cm^3 g^{-1}) were larger than the diameter of the MB molecule (4.3 × 5.0 × 13.9 Å),[38] revealing the high potential for the adsorption of MB into the pores of biochar.[19] The SSA of $NaCBC_{300}$ decreased as compared to that of CBC_{300}, which might be attributed to the collapse of pore walls or the occupancy of interstitial pores by NaOH.[39–41] The modification process might eliminate pore-blocking substances (*e.g.*, hemicellulose and lignin) and lead to the formation of additional pores, which would increase pore volume and therefore enhance the adsorption ability.[42,43] Pyrolysis temperature greatly affected the SSA, TPV, and AP of CBCs (Table S3†). SSA of CBC_{600} (187.1 m^2 g^{-1}) was 1.2 and 1.1 folds higher than those of CBC_{400} and CBC_{500}, respectively. Because of the volatilization and loss of macromolecules in the biomass, larger SSA of CBC_{400}, CBC_{500}, and CBC_{600} (148.9, 169.6, and 187.1 m^2 g^{-1}) was obtained with higher pyrolysis temperatures of 400, 500, and 600 °C, respectively, which led to a greater quantity of pores within the biochar matrix.[44]

XRD patterns of CBC_{300}, CBC_{400}, CBC_{500}, CBC_{600}, and $NaCBC_{300}$ were presented in Fig. 1c. The spectra of these five biochars revealed two peaks at 2θ = 26° and 43°, which respectively corresponded to quartz (SiO_2) and the (100) plane of crystalline carbons. Additionally, a diffraction peak at 2θ = 23° which was assigned to the (002) plane of amorphous carbons was detected in the XRD spectra of CBC and NaCBC systems.[45]

Functional groups of CBC_{300} and $NaCBC_{300}$ were revealed by FTIR spectroscopy (Fig. 1d and Table S4†). The peak intensity at 3408 cm^{-1} corresponded to –OH stretching vibration in the spectra of $NaCBC_{300}$ was higher than that in the CBC_{300} spectra, indicating the higher contents of –OH in $NaCBC_{300}$.[33] This might be conducive to the adsorption of MB molecules due to the high polarization of –OH.[33] The peak at 2930 cm^{-1} was attributed to C–H stretching vibration of the methylene groups.[46] Two bands at about 2359 and 670 cm^{-1} could be assigned to CO_2 species.[47] The peak at near 1700 cm^{-1} indicated C=O stretch of ketones, aldehydes, and esters,[48] while the peaks around 1609–1632 cm^{-1} might be assigned to C=N, C=O, or C=C bonds in aromatic rings. Moreover, the peaks at 1531 and 1444–1448 cm^{-1} represented the stretching vibration of C=C in lignin and aromatic C=O and C=C, respectively. The contents of surface functional groups decreased with the increase of pyrolysis temperature, potentially as a consequence of the decomposition of the macromolecules.[36] According to earlier researches, absorbents rich in aromatics might be conducive to the adsorption of hydrophobic organic compounds.[19,49] The increasing content of –OH in $NaCBC_{300}$ may form a hydrogen bond with the aromatic ring of MB,[50] and the changes in aromatic C=O and C=C bonds indicated that there may be a π–π bond between the aromatic ring structures of $NaCBC_{300}$ and MB.[51]

The strong C 1s peak in both CBC_{300} and $NaCBC_{300}$ spectra manifested that carbon element was dominant in the biochar samples (Fig. 1e). The C 1s XPS spectra of CBC_{300} and $NaCBC_{300}$ could be deconvoluted into five peaks at 284.00, 284.63, 288.50, 286.85, and 285.62 eV, which were assigned to C=C, C–C, C–N, C–O, and C=O, respectively (Fig. 1f). Notably, a new peak of C–Na at 285.62 eV appeared in the spectrum of $NaCBC_{300}$, indicating the doping of Na during NaOH modification. XPS O 1s spectrum of CBC_{300} at near 532.79 and 531.40 eV could be ascribed to C=O and C–O, respectively. In addition to these functional groups, a new peak at 532.08 eV corresponding to –OH was shown in the spectrum of $NaCBC_{300}$ (Fig. 1g). XPS N 1s spectrum at near 400.23 and 398.93 eV could be allocated to C–N and –NH, respectively (Fig. 1h). The peak of XPS Na 1 s

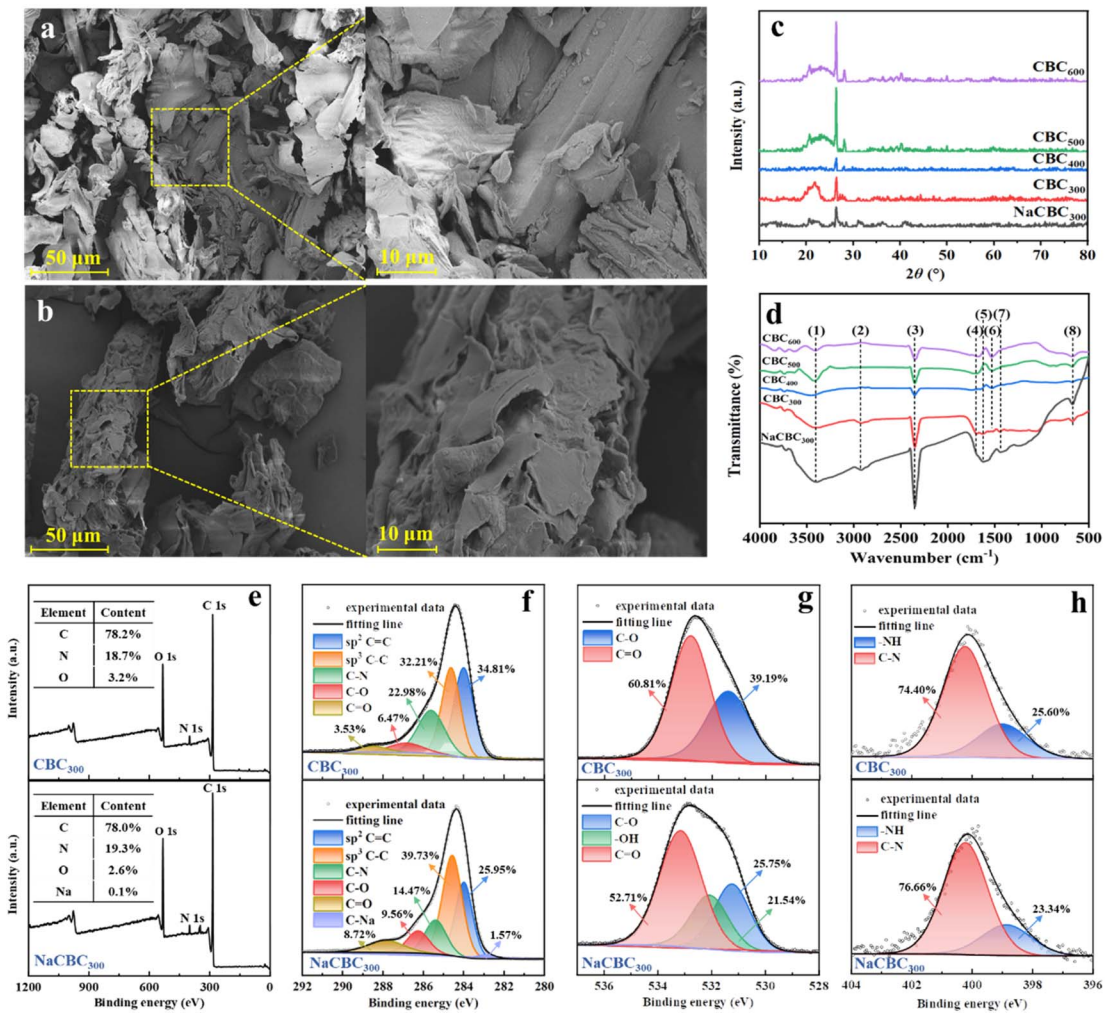

Fig. 1 Characterization of biochars. SEM observations of (a) CBC_{300} and (b) $NaCBC_{300}$, (c) XRD patterns, (d) FTIR spectra and (e–h) XPS (e) survey, (f) C 1s, (g) O 1s, and (h) N 1s spectra of CBC and $NaCBC_{300}$. Peak (1)–(8) in the FTIR spectra indicated –OH, C–H, CO_2, C=O, C=O in aromatic rings, C=C, aromatic C=O and C=C, and CO_2, respectively. Detailed locations, assignments, and references of the FTIR peaks were provided in Table S4.†

might be sodium silicates since silica was commonly observed in many cereal plants including rice, wheat, and corn (Fig. S5†).[52] In addition to the common functional groups for CBCs, $NaCBC_{300}$ exhibited stronger peaks of –OH and C=C at 3408 and 1609 cm^{-1}, respectively. This was consistent with the earlier FTIR results[40] and suggested that these functional groups were implicated in the significant increase in MB adsorption onto the $NaCBC_{300}$ through chemisorption.[50,53]

3.2 Optimal performance of MB adsorption on biochars

3.2.1 Effects of modification and pyrolysis temperatures. As shown in Fig. S6,† limited MB removal by pristine corn straw and NaOH-modified corn straw was demonstrated (<10%). Compared with the biomass without pyrolysis, biochar possesses a rich void structure and chemical groups distributed on its surface,[54] which would result in eminent adsorption ability. With the initial MB concentration of 100 mg L^{-1}, $NaCBC_{300}$ was capable of removing 99.9% of MB, which was 1.1–74.4% higher than the other 16 control samples (Table S1†). Moreover, investigations on the removal efficiency and adsorption capacity of CBCs and NaCBCs produced at various pyrolysis temperatures were conducted (Fig. 2). About 34.8%, 6.9%, 10.2%, and 26.1% of MB was adsorbed by CBC_{300}, CBC_{400}, CBC_{500}, and CBC_{600}, respectively (Fig. 2a). The removal efficiencies of MB by NaCBCs were 63.6%, 47.0%, 25.8%, and 67.6% higher than those by CBC possessing the same pyrolysis temperature (*i.e.*, 300, 400, 500, and 600 °C), respectively. When the pyrolysis temperature was increased from 300 to 500 °C, the adsorption capacity of NaCBCs gradually decreased from 49.2 to 18.0 mg L^{-1}. Additionally, the adsorption capacity of NaCBC was increased to 46.8 mg L^{-1} when the pyrolysis temperature was further increased to 600 °C. The adsorption capacity of CBC with different pyrolysis temperatures revealed a similar trend to that of NaCBCs, with MB removals of 17.4, 3.4, 5.1, and 13.1 mg L^{-1} when the pyrolysis temperatures were 300, 400, 500, and 600 °C, respectively (Fig. 2b). As validated by FTIR spectra (Fig. 1d and Table S5†), the decrease of functional groups of CBCs with the increase of pyrolysis temperature (300–500 °C)

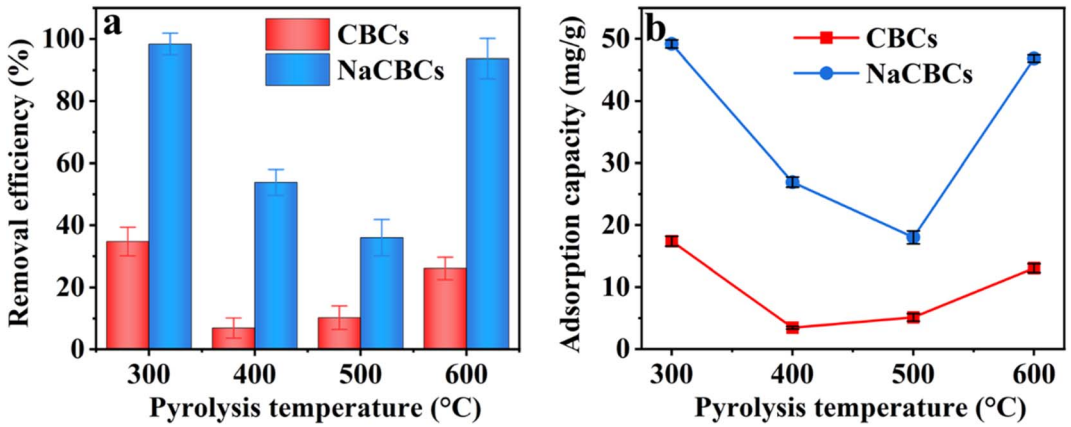

Fig. 2 MB (100 mg L^{-1}) (a) removal efficiency and (b) adsorption capacity by CBCs and NaCBCs with different pyrolysis temperatures.

might be the reason for the decline in removal ability. Furthermore, the enhancement in SSA from 1.16 to 4.61 m^2 g^{-1} with the pyrolysis temperature from 300 to 600 °C could be responsible for the improved adsorption ability at 600 °C (Table S3†).

3.2.2 Effects of biochar dosage and MB concentration on adsorption. The biochar dosage greatly influenced the adsorbent–adsorbate equilibrium,[55] and the initial concentration of dye offered a driving force to promote the mass transfer of dye molecules.[56] Therefore, the effects of the adsorbent dosages (0.02–0.10 g L^{-1}) and initial MB concentration (50–250 mg L^{-1}) on MB adsorption were investigated (Fig. 3).

The dosages of CBC_{300} and $NaCBC_{300}$ varied from 0.02 to 0.10 g L^{-1} at the initial MB concentration of 50 mg L^{-1}, the removal efficiency by CBC_{300} was considerably increased from 21.8% to 77.5%; higher MB removal efficiency (99.3–100.0%) was shown during the adsorption by $NaCBC_{300}$. Additionally, when the initial MB concentration was boosted from 100 to 250 mg L^{-1}, the removal efficiency of CBC_{300} increased from 12.9% to 34.0%, and the efficiency significantly increased from 46.5% to 99.1% in the $NaCBC_{300}$ mediated system (Fig. 3a and b).

With the increase of CBC_{300} dosage from 0.02 to 0.06 g L^{-1}, the adsorption capacity of MB (50 mg L^{-1}) by CBC_{300} was improved from 27.3 to 63.1 mg g^{-1}, and eventually decreased to 46.86 mg g^{-1} with the dosage of 0.10 g L^{-1}. When initial MB concentrations were increased from 100 to 250 mg L^{-1}, the adsorption capacity of MB decreased with the increase of CBC_{300} dosages. At the dosage of 0.02 g L^{-1}, the adsorption capacity of MB (250 mg L^{-1}) by $NaCBC_{300}$ (290.71 mg g^{-1}) was about three folds greater than that by CBC_{300}. With the biochar dosages of 0.04, 0.06, 0.08, and 0.10 g L^{-1}, the adsorption capacity of MB (250 mg L^{-1}) by $NaCBC_{300}$ (221.7, 182.3, 151.5, and 123.9 mg g^{-1}) were four times higher than those by CBC_{300}, respectively (Fig. 3c and d). Higher adsorbent dosages with lower adsorption capacities were found, which could be due to the availability of more adsorption sites at higher dosages. The formation of aggregation of particles were induced, thereby exposing limited active sites for efficient adsorption.[33,57]

After NaOH modification, the removal efficiency and adsorption capacity of $NaCBC_{300}$ were significantly improved to 100.0% and 290.7 mg g^{-1}, respectively. The adsorption capacities of several reported low-cost waste biomass toward MB adsorption were summarized in Table 1. Compared with these reported materials, $NaCBC_{300}$ exhibited excellent adsorption capacity, indicating that it was a promising adsorbent for dye removal. After five cycles, over 70% of MB could still be removed by $NaCBC_{300}$, indicating its high reusability (Fig. S7†).

3.3 Adsorption isotherm

The equilibrium adsorption isotherm could be described well by different isotherm models to explain the interaction between adsorbate and adsorbent (Fig. 4 and Table S6†).[63] The adsorption isotherms of MB adsorbed by $NaCBC_{300}$ have been fitted with all the equilibrium data in Fig. 4. The correlation coefficient value of Freundlich isotherm model ($R^2 = 0.92$) was higher than that of Langmuir isotherm model ($R^2 = 0.89$), indicating that the Freundlich isotherm model was more suitable for the isothermal behavior during the adsorption process. This result demonstrated that multilayer adsorption was more inclined to be the equilibrium adsorption mechanism of MB by $NaCBC_{300}$.[64] Besides, it could be inferred that the surface of $NaCBC_{300}$ was heterogenous, on which MB molecules were adsorbed with multilayer.[65]

3.4 Potential adsorption mechanisms of MB on $NaCBC_{300}$

Adsorptive properties of organic chemicals on adsorbents were generally determined by their physical and chemical interaction. Multiple researches have indicated that the removal of pollutants from water by biochar was a complex process. A variety of factors, including porous structure, π–π interaction, charged surface, surface functional groups, and hydrogen bonding force, have been revealed to influence dye adsorption by biochar.[40,43,66] For instance, Jawad *et al.* reported that the covalent forces generated by the sharing of electrons between pollutants and adsorbents were in control of the pace of chemical adsorption.[67] According to the investigations of Shao *et al.*, the dominant mechanisms for the adsorption of cationic dyes were complexation and electrostatic attractions between oxygen-containing functional groups of the chemically modified adsorbent and dye molecules.[68]

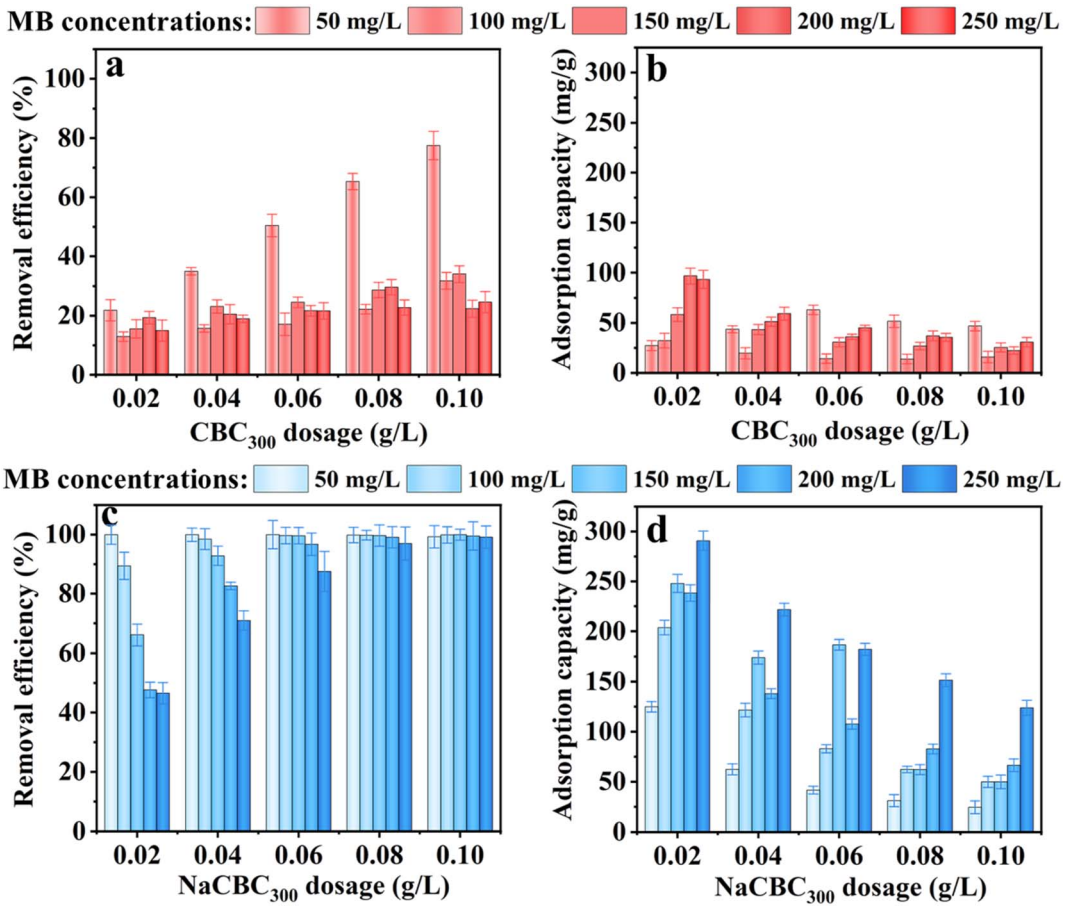

Fig. 3 Removal efficiency and adsorption capacity of MB by (a and b) CBC_{300} and (c and d) $NaCBC_{300}$ with different biochar dosages and MB concentrations.

Table 1 Comparison of adsorption capacity of NaOH-modified biochars for MB adsorption

Biochars	Adsorption capacity ($mg\ g^{-1}$)	Ref.
Cotton residue	23.82	58
Spent auricularia auricula substrate	53.62	59
Tea residue	105.27	56
Sugarcane bagasse	114.42	60
Sludge derived biochar	160.78	61
Wheat straw	250.30	62
$NaCBC_{300}$	290.71	This work

In this study, DFT calculations were conducted to gain insight into the adsorption mechanisms and potential sites *via* Materials Studio DMol3 version 8.0.[69,70] Geometric optimization and energy calculation were done using generalized gradient approximation (GGA) within the Becke exchange plus Lee–Yang–Parr correlation (BLYP). The interaction between $NaCBC_{300}$ and MB was calculated, the adsorption energy (ΔE_{ad}) between the $NaCBC_{300}$ and the MB was calculated according to the eqn (5):

$$\Delta E_{ad} = E_{total} - E_{NaCBC_{300}} - E_{MB} \quad (5)$$

where, E_{total} was the total energy of the interaction between $NaCBC_{300}$ and MB; $E_{NaCBC_{300}}$ was the energy of $NaCBC_{300}$; E_{MB} was the energy of MB molecule.

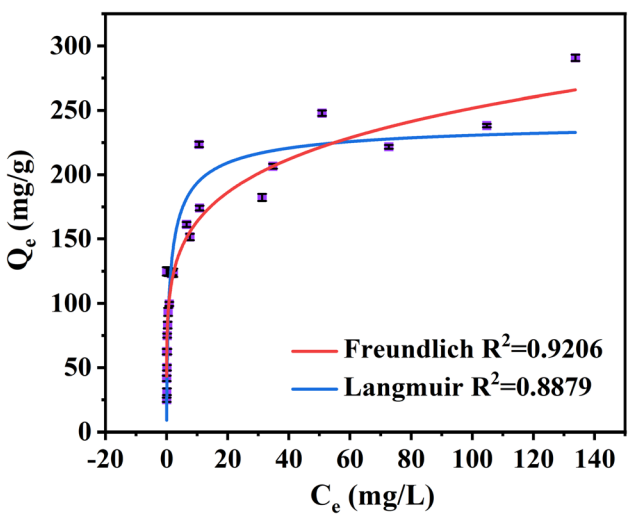

Fig. 4 Adsorption isotherms of MB adsorbed by $NaCBC_{300}$.

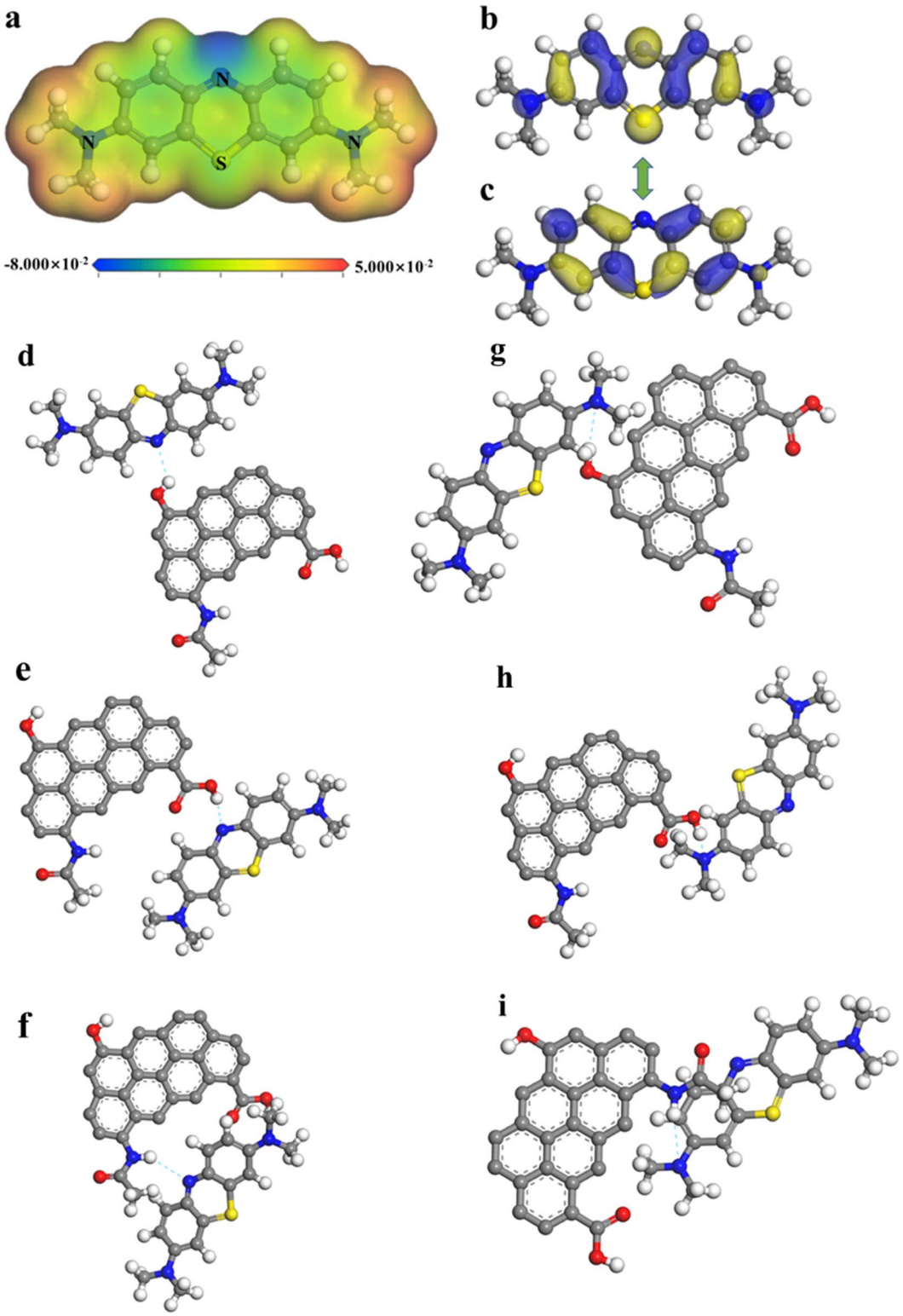

Fig. 5 (a) MEP of MB and interaction mechanism of MB with $NaCBC_{300}$ based on (b) HOMO and (c) LUMO, and (g–i) configuration of interactions between $NaCBC_{300}$ and MB: (d) –OH–N1, (e) –COOH–N1, (f) –NH–N1, (g) –OH–N2, (h) –COOH–N2, (i) –NH–N2, (gray, white, blue, and yellow balls denoted C, H, N, and S atoms, respectively).

In the molecular electrostatic potentials (MEP) of MB, the region of upper and lower potential (represented by red and blue colors, respectively) represented potential sites of attack (Fig. 5a).[71] Furthermore, the concept of the Fukui function was crucial to conceptual density functional theory (CDFT), which has been extensively applied to predict the reactive sites for

Table 2 Interaction site, bond length, and adsorption energy between $NaCBC_{300}$ and MB

Interaction site	Bond length (Å)	ΔE_{ad} (eV)
–OH–N1	2.104	−0.1294
–COOH–N1	2.141	−0.0888
–NH–N1	2.853	−0.0723
–OH–N2	2.108	−0.1089
–COOH–N2	1.483	−0.3365
–NH–N2	3.092	−0.0296

nucleophilic, electrophilic, and radical attacks.[72] To investigate the mechanism in depth, the charge distribution and Fukui function representing electrophilic (f^-), nucleophilic (f^+), and general radical (f^0) attack of the atoms on MB molecule were calculated and displayed in Fig. S8.†[73,74] The phenothiazine nitrogen atom was at a lower potential (represented as blue), and could be a target for electrophilic attack, whereas the atoms of dimethylamine benzene were at a higher potential (represented as red), could be a target for nucleophilic assault.[72] The results of the MEP analyses showed that the nitrogen and the dimethylamine group of MB interacted in an electrophilic and nucleophilic manner, respectively.

The interaction mechanism was explored by calculating the highest occupied molecular orbital (HOMO) and lowest unoccupied molecular orbital (LUMO) of MB based on the frontier molecular orbital theory (Fig. 5b and c), which revealed the ability to accept or donate electrons on active sites and determined the tendency of chemical reaction (Table S7†).[75] Previous studies have proposed that the π electron donor–acceptor interaction was an adsorption mechanism involving π electrons in both the adsorbent and adsorbate. In biochar, functional groups like amines and methyl served as the π electron donors, and in MB, R–$N(CH_3)_2$ groups served as the π electron acceptors.[71,76]

To provide a clearer description of the interaction strength between $NaCBC_{300}$ and MB, different interaction conformations were defined through DFT calculations, and the adsorption energy was calculated (Table 2 and Fig. 5d–i). The shorter bond length demonstrated the stronger the interaction force. ΔE_{ad} were all negative for $NaCBC_{300}$ MB models, which indicated the favorable spontaneous adsorption of MB on $NaCBC_{300}$. From the perspective of adsorption energy, the smaller of adsorption energy, the more conducive to adsorption, and the trend of ΔE_{ad} proved that –COOH and –OH were the main adsorption functional groups. The most possibility of the attraction between $NaCBC_{300}$ and MB model was between –COOH in $NaCBC_{300}$ and R–$N(CH_3)_2$ in MB. The order of preferable interaction between MB and the functional groups in $NaCBC_{300}$ were as follow: –COOH > –OH > –NH.

In this study, changes in C=C and C=O bonds indicated that the π–π interaction between aromatic rings of MB (π-acceptor) and $NaCBC_{300}$ (π-donor) were formed during the adsorption process based on FTIR analyses.[77,78] Additionally, XPS analyses clearly showed the change in $NaCBC_{300}$ surface with a new band of –OH, which suggested the formation of H-bonding between biochar and aromatic ring of MB.[77] Besides,

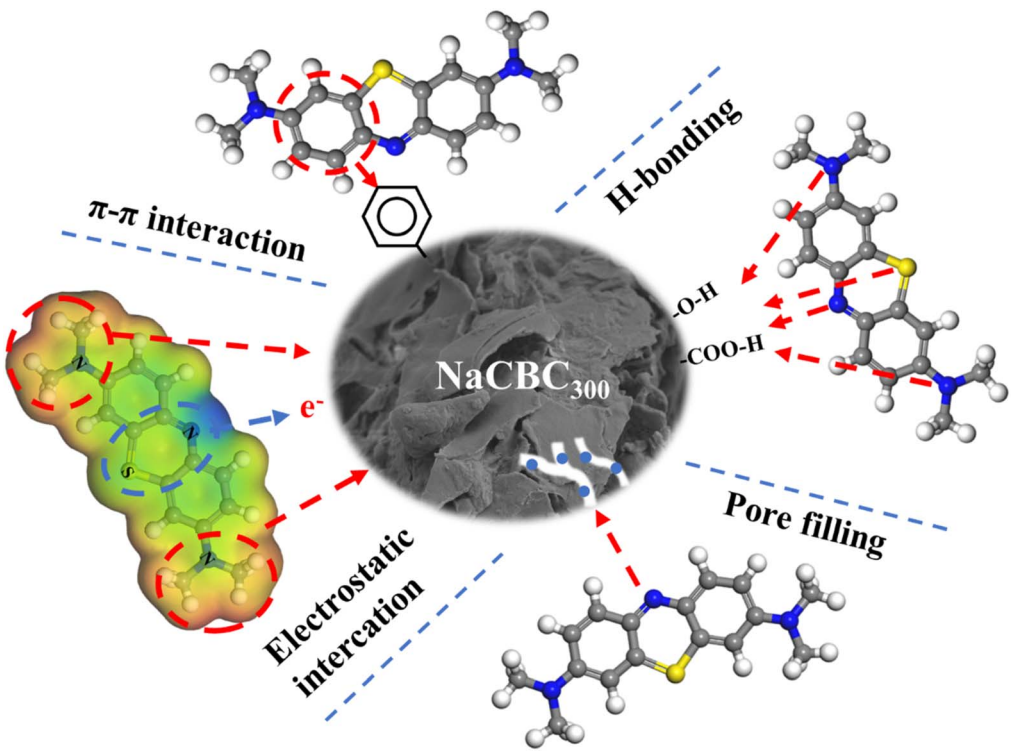

Fig. 6 Schematic diagram of the adsorption mechanism between MB and $NaCBC_{300}$.

the stronger MB adsorption on $NaCBC_{300}$ than CBC_{300} appeared to be attributable to the change of surface properties upon alkaline treatment, which was conducive to the adsorption process. Results of SEM and BET showed that $NaCBC_{300}$ possessed more fine holes than CBC_{300}, indicating pore-filling effect due to the larger pore volume of MB adsorption affinity on $NaCBC_{300}$ (Fig. 6). Therefore, the adsorption mechanisms included π–π interaction, H-bonding, electrostatic interaction, and pore-filling between $NaCBC_{300}$ and MB.

4. Conclusion

$NaCBC_{300}$ was successfully synthesized and revealed as an effective adsorbent for the removal of MB from wastewater. Adsorption isotherm was better fitted by the Freundlich, suggesting multilayer adsorption played a dominant role in the adsorption of MB. FTIR and XPS analyses demonstrated that the adsorption between biochar and MB mainly interacted through π–π interaction and H-bonding. Results of SEM and BET showed that pore-filling effects also played significant roles in MB adsorption. Based on DFT calculations, the mechanism of electrostatic interaction and reactive sites of $R–N(CH_3)_2$ groups in MB were predicted by the ways of MEP, HOMO, and LUMO. This study not only provided an alternative way for the reuse of waste corn straw but also demonstrated an efficient and cost-effective adsorbent for wastewater treatment.

Conflicts of interest

There are no conflicts to declare.

Acknowledgements

This work was supported by the National Natural Science Foundation of China (No. 42207288), the Doctoral Scientific Research Foundation of Liaoning Province (No. 2023-BS-172), the Dalian Science and Technology Talent Innovation Support Plan (No. 2022RQ032), the Open Project of Key Laboratory of Agro-Forestry Environmental Processes and Ecological Regulation of Hainan Province (Hainan University, No. AFEPER202201), the Open Foundation of Key Laboratory of Industrial Ecology and Environmental Engineering (MOE, No. KLIEEE-22-08), and the Basic scientific research project of Liaoning Provincial Department of Education (JYTQN2023006).

References

1 S. Dutta, B. Gupta, S. K. Srivastava and A. K. Gupta, Recent advances on the removal of dyes from wastewater using various adsorbents: a critical review, *Mater. Adv.*, 2021, **2**, 4497–4531.

2 C. J. Ogugbue and T. Sawidis, Bioremediation and detoxification of synthetic wastewater containing triarylmethane dyes by Aeromonas hydrophila isolated from industrial effluent, *Biotechnol. Res. Int.*, 2011, **2011**, 967925.

3 A. L. D. Da Rosa, E. Carissimi, G. L. Dotto, H. Sander and L. A. Feris, Biosorption of rhodamine B dye from dyeing stones effluents using the green microalgae Chlorella pyrenoidosa, *J. Cleaner Prod.*, 2018, **198**, 1302–1310.

4 N. Ertugay and F. N. Acar, Removal of COD and color from Direct Blue 71 azo dye wastewater by Fenton's oxidation: Kinetic study, *Arabian J. Chem.*, 2017, **10**, S1158–S1163.

5 V. Katheresan, J. Kansedo and S. Y. Lau, Efficiency of various recent wastewater dye removal methods: A review, *J. Environ. Chem. Eng.*, 2018, **6**, 4676–4697.

6 M. Bilal, I. Ihsanullah, S. M. Hassan, R. A. Bhaskar and T. M. Aminabhavi, Recent advances in the removal of dyes from wastewater using low-cost adsorbents, *J. Environ. Manage.*, 2022, **321**, 115981.

7 K. P. Gopinath, D. N. Vo, D. Gnana Prakash, A. Adithya Joseph, S. Viswanathan and J. Arun, Environmental applications of carbon-based materials: A review, *Environ. Chem. Lett.*, 2021, **19**, 557–582.

8 E. Santoso, R. Ediati, Y. Kusumawati, H. Bahruji, D. O. Sulistiono and D. Prasetyoko, Review on recent advances of carbon based adsorbent for methylene blue removal from waste water, *Mater. Today Chem.*, 2020, **16**, 100233.

9 A. Kheddo, L. Rhyman, M. I. Elzagheid, P. Jeetah and P. Ramasami, Adsorption of synthetic dyed wastewater using activated carbon from rice husk, *SN Appl. Sci.*, 2020, **2**, 2170.

10 A. Gupta, H. Viltres and N. K. Gupta, Sono-adsorption of organic dyes onto CoFe2O4/graphene oxide nanocomposite, *Surf. Interfaces*, 2020, **20**, 100563.

11 G. Song, A. Li, Y. Shi, W. Li, H. Wang, C. Wang, R. Li and G. Ding, Sorptive removal of methylene blue from water by magnetic multi-walled carbon nanotube composites, *Environ. Sci. Pollut. Res. Int.*, 2021, **28**, 41268–41282.

12 M. Jain, S. A. Khan, A. Sahoo, P. Dubey, K. K. Pant, Z. M. Ziora and M. A. T. Blaskovich, Statistical evaluation of cow-dung derived activated biochar for phenol adsorption: Adsorption isotherms, kinetics, and thermodynamic studies, *Bioresour. Technol.*, 2022, **352**, 127030.

13 B. Qiu, X. Tao, H. Wang, W. Li, X. Ding and H. Chu, Biochar as a low-cost adsorbent for aqueous heavy metal removal: A review, *J. Anal. Appl. Pyrolysis*, 2021, **155**, 105081.

14 A. Kumar, T. Bhattacharya, W. A. Shaikh, S. Chakraborty, D. Sarkar and J. K. Biswas, Biochar modification methods for augmenting sorption of contaminants, *Curr. Pollut. Rep.*, 2022, **8**, 519–555.

15 I. Herath, P. Kumarathilaka, M. I. Al-Wabel, A. Abduljabbar, M. Ahmad, A. R. A. Usman and M. Vithanage, Mechanistic modeling of glyphosate interaction with rice husk derived engineered biochar, *Microporous Mesoporous Mater.*, 2016, **225**, 280–288.

16 D. Mohan, A. Sarswat, Y. S. Ok and C. U. Pittman, Organic and inorganic contaminants removal from water with biochar, a renewable, low cost and sustainable adsorbent-A critical review, *Bioresour. Technol.*, 2014, **160**, 191–202.

17 M. Vithanage, S. S. Mayakaduwa, I. Herath, Y. S. Ok and D. Mohan, Kinetics, thermodynamics and mechanistic studies of carbofuran removal using biochars from tea waste and rice husks, *Chemosphere*, 2016, **150**, 781–789.
18 R. Zhao, N. Coles, Z. Kong and J. Wu, Effects of aged and fresh biochars on soil acidity under different incubation conditions, *Soil Tillage Res.*, 2015, **146**, 133–138.
19 N. X. Cuong, H. N. T. Thanh, C. N. T. Hong, Q. Van Le, B. V. T. Yen, P. T. T. Cuc, L. D. Duong, G. Kumar, N. V. Khanh, S. W. Chang, C. W. Jin and D. Duc Nguyen, Sustainable carbonaceous biochar adsorbents derived from agro-wastes and invasive plants for cation dye adsorption from water, *Chemosphere*, 2021, **282**, 131009.
20 T. Suwunwong, N. Hussain, S. Chantrapromma and K. Phoungthong, Facile synthesis of corncob biochar via in-house modified pyrolysis for removal of methylene blue in wastewater, *Mater. Res. Express*, 2020, **7**, 15518.
21 B. Chen, Z. Chen and S. Lv, A novel magnetic biochar efficiently sorbs organic pollutants and phosphate, *Bioresour. Technol.*, 2011, **102**, 716–723.
22 J. H. Park, Y. S. Ok, S. H. Kim, J. S. Cho, J. S. Heo, R. D. Delaune and D. C. Seo, Evaluation of phosphorus adsorption capacity of sesame straw biochar on aqueous solution: Influence of activation methods and pyrolysis temperatures, *Environ. Geochem. Health*, 2015, **37**, 969–983.
23 K. A. Krishnan and A. Haridas, Removal of phosphate from aqueous solutions and sewage using natural and surface modified coir pith, *J. Hazard. Mater.*, 2008, **152**, 527–535.
24 M. A. Lillo-Ródenas, D. Cazorla-Amorós and A. Linares-Solano, Understanding chemical reactions between carbons and NaOH and KOH, *Carbon*, 2003, **41**, 267–275.
25 L. Du, S. Ahmad, L. Liu, L. Wang and J. Tang, A review of antibiotics and antibiotic resistance genes (ARGs) adsorption by biochar and modified biochar in water, *Sci. Total Environ.*, 2023, **858**, 159815.
26 X. Jing, Y. Wang, W. Liu, Y. Wang and H. Jiang, Enhanced adsorption performance of tetracycline in aqueous solutions by methanol-modified biochar, *Chem. Eng. J.*, 2014, **248**, 168–174.
27 Y. Fan, B. Wang, S. Yuan, X. Wu, J. Chen and L. Wang, Adsorptive removal of chloramphenicol from wastewater by NaOH modified bamboo charcoal, *Bioresour. Technol.*, 2010, **101**, 7661–7664.
28 H. Wang, J. Xu and L. Sheng, Preparation of straw biochar and application of constructed wetland in China: A review, *J. Cleaner Prod.*, 2020, **273**, 123131.
29 S. Majidian, M. Afsharnia, M. Taghavi, N. Afshar Kohan and A. Dehghan, Photocatalytic degradation of methylene blue dye using bismuth oxyiodide from aqueous solutions, *Int. J. Environ. Anal. Chem.*, 2022, 1–13.
30 Y. Mittal, S. Dash, P. Srivastava, P. M. Mishra, T. M. Aminabhavi and A. K. Yadav, Azo dye containing wastewater treatment in earthen membrane based unplanted two chambered constructed wetlands-microbial fuel cells: A new design for enhanced performance, *Chem. Eng. J.*, 2022, **427**, 131856.
31 M. Esen and T. Yuksel, Experimental evaluation of using various renewable energy sources for heating a greenhouse, *Energy Build.*, 2013, **65**, 340–351.
32 Y. Wang, J. Luo, J. Qin, Y. Huang, T. Ke, Y. Luo and M. Yang, Efficient removal of phytochrome using rice straw-derived biochar: Adsorption performance, mechanisms, and practical applications, *Bioresour. Technol.*, 2023, **376**, 128918.
33 S. Xue, B. Tu, Z. Li, X. Ma, Y. Xu, M. Li, C. Fang and H. Tao, Enhanced adsorption of Rhodamine B over Zoysia sinica Hance-based carbon activated by amminium chloride and sodium hydroxide treatments, *Colloids Surf., A*, 2021, **618**, 126489.
34 X. Liu, J. Sun, S. Duan, Y. Wang, T. Hayat, A. Alsaedi, C. Wang and J. Li, A valuable biochar from poplar catkins with high adsorption capacity for both organic pollutants and inorganic heavy metal ions, *Sci. Rep.*, 2017, **7**, 10033.
35 C. Cui, M. Yang, J. Zhai, W. Bai, L. Dai, L. Liu, S. Jiang, W. Wang, E. Ren, C. Cheng and R. Guo, Bamboo cellulose-derived activated carbon aerogel with controllable mesoporous structure as an effective adsorbent for tetracycline hydrochloride, *Environ. Sci. Pollut. Res.*, 2023, **30**, 12558–12570.
36 B. Biswas, P. Balla, B. B. Krishna, A. Sushil and T. Bhaskar, Physiochemical characteristics of bio-char derived from pyrolysis of rice straw under different temperatures, *Biomass Convers. Biorefin.*, 2022, DOI: **10.1007/s13399-022-03261-y**.
37 Z. Jin, S. Xiao, H. Dong, J. Xiao, R. Tian, J. Chen, Y. Li and L. Li, Adsorption and catalytic degradation of organic contaminants by biochar: Overlooked role of biochar's particle size, *J. Hazard. Mater.*, 2022, **422**, 126928.
38 Y. Shi, Q. Chang, T. Zhang, G. Song, Y. Sun and G. Ding, A review on selective dye adsorption by different mechanisms, *J. Environ. Chem. Eng.*, 2022, **10**, 108639.
39 N. Chaukura, E. C. Murimba and W. Gwenzi, Synthesis, characterisation and methyl orange adsorption capacity of ferric oxide-biochar nano-composites derived from pulp and paper sludge, *Appl. Water Sci.*, 2017, **7**, 2175–2186.
40 D. Nguyen, Q. A. Binh, X. C. Nguyen, N. T. Huyen, Q. N. Vo, T. D. Nguyen, T. T. Phuong, N. T. Hang, S. Y. Kim, T. P. Nguyen, J. Bae, I. T. Kim and Q. Van Le, Metal salt-modified biochars derived from agro-waste for effective congo red dye removal, *Environ. Res.*, 2021, **200**, 111492.
41 F. Rodríguez-Reinoso and M. Molina-Sabio, Textural and chemical characterization of microporous carbons, *Adv. Colloid Interface Sci.*, 1998, **76**, 271–294.
42 M. Kelm, S. J. M. Da, H. S. de Barros, C. de Araujo, F. R. de Assis, E. J. Freitas, S. D. Dos and M. S. M. Da, Removal of azo dye from water via adsorption on biochar produced by the gasification of wood wastes, *Environ. Sci. Pollut. Res.*, 2019, **26**, 28558–28573.
43 S. Sutar, P. Patil and J. Jadhav, Recent advances in biochar technology for textile dyes wastewater remediation: A review, *Environ. Res.*, 2022, **209**, 112841.
44 A. E. de Castro, F. Da Silva Martinho, M. L. Barbosa, J. R. Franca, J. Ribeiro-Soares, G. M. D. Ferreira and G. M. D. Ferreira, Influence of methyl groups in

triphenylmethane dyes on their adsorption on biochars from coffee husks, *Water, Air, Soil Pollut.*, 2022, **233**, 180.
45 C. Hung, C. Huang, J. Cheng, C. Chen and C. Dong, Production and characterization of a high value-added seaweed-derived biochar: Optimization of pyrolysis conditions and evaluation for sediment treatment, *J. Anal. Appl. Pyrolysis*, 2021, **155**, 105071.
46 F. Ma, J. Dai, Z. Fu, C. Li, Y. Wen, M. Jia, Y. Wang and K. Shi, Biochar for asphalt modification: A case of high-temperature properties improvement, *Sci. Total Environ.*, 2022, **804**, 150194.
47 M. Al-Wabel, J. Elfaki, A. Usman, Q. Hussain and Y. S. Ok, Performance of dry water- and porous carbon-based sorbents for carbon dioxide capture, *Environ. Res.*, 2019, **174**, 69–79.
48 A. Tomczyk, Z. Sokołowska and P. Boguta, Biochar physicochemical properties: Pyrolysis temperature and feedstock kind effects, *Rev. Environ. Sci. Biotechnol.*, 2020, **19**, 191–215.
49 L. Han, L. Qian, J. Yan and M. Chen, Effects of the biochar aromaticity and molecular structures of the chlorinated organic compounds on the adsorption characteristics, *Environ. Sci. Pollut. Res.*, 2017, **24**, 5554–5565.
50 J. Chen, C. Tang, X. Li, J. Sun, Y. Liu, W. Huang, A. Wang and Y. Lu, Preparation and modification of rape straw biochar and its adsorption characteristics for methylene blue in water, *Water*, 2022, **14**, 3761.
51 Z. Xu, Y. Xiang, H. Zhou, J. Yang, Y. He, Z. Zhu and Y. Zhou, Manganese ferrite modified biochar from vinasse for enhanced adsorption of levofloxacin: Effects and mechanisms, *Environ. Pollut.*, 2021, **272**, 115968.
52 M. N. Nguyen, Potential use of silica-rich biochar for the formulation of adaptively controlled release fertilizers: A mini review, *J. Cleaner Prod.*, 2021, **307**, 127188.
53 N. Li, M. Yin, D. C. W. Tsang, S. Yang, J. Liu, X. Li, G. Song and J. Wang, Mechanisms of U(VI) removal by biochar derived from Ficus microcarpa aerial root: A comparison between raw and modified biochar, *Sci. Total Environ.*, 2019, **697**, 134115.
54 D. L. T. Nguyen, Q. A. Binh, X. C. Nguyen, T. T. Huyen Nguyen, Q. N. Vo, T. D. Nguyen, T. C. Phuong Tran, T. A. Hang Nguyen, S. Y. Kim, T. P. Nguyen, J. Bae, I. T. Kim and Q. Van Le, Metal salt-modified biochars derived from agro-waste for effective congo red dye removal, *Environ. Res.*, 2021, **200**, 111492.
55 L. Goswami, A. Kushwaha, S. R. Kafle and B. Kim, Surface modification of biochar for dye removal from wastewater, *Catalysts*, 2022, **12**, 817.
56 Y. Mu and H. Ma, NaOH-modified mesoporous biochar derived from tea residue for methylene Blue and Orange II removal, *Chem. Eng. Res. Des.*, 2021, **167**, 129–140.
57 G. Prasannamedha, P. S. Kumar, R. Mehala, T. J. Sharumitha and D. Surendhar, Enhanced adsorptive removal of sulfamethoxazole from water using biochar derived from hydrothermal carbonization of sugarcane bagasse, *J. Hazard. Mater.*, 2021, **407**, 124825.
58 C. T. Primaz, A. Ribes-Greus and R. A. Jacques, Valorization of cotton residues for production of bio-oil and engineered biochar, *Energy*, 2021, **235**, 121363.
59 L. Su, H. Zhang, K. Oh, N. Liu, Y. Luo, H. Cheng, G. Zhang and X. He, Activated biochar derived from spent Auricularia auricula substrate for the efficient adsorption of cationic azo dyes from single and binary adsorptive systems, *Water Sci. Technol.*, 2021, **84**, 101–121.
60 A. E. Moharm, N. G. El, H. Soliman, A. I. Abd-Elhamid, A. A. El-Bardan, T. S. Kassem, A. A. Nayl and S. Brase, Fabrication and characterization of effective biochar biosorbent derived from agricultural waste to remove cationic dyes from wastewater, *Polymers*, 2022, **14**, 2587.
61 I. I. Shahib, J. Ifthikar, D. T. Oyekunle, Z. Elkhlifi, A. Jawad, J. Wang, W. Lei and Z. Chen, Influences of chemical treatment on sludge derived biochar; Physicochemical properties and potential sorption mechanisms of lead (II) and methylene blue, *J. Environ. Chem. Eng.*, 2022, **10**, 107725.
62 S. M. Sodkouieh, M. Kalantari and T. Shamspur, Methylene blue adsorption by wheat straw-based adsorbents: Study of adsorption kinetics and isotherms, *Korean J. Chem. Eng.*, 2023, **40**, 873–881.
63 X. Li, T. Gan, J. Zhang, Z. Shi, Z. Liu and Z. Xiao, High-capacity removal of oxytetracycline hydrochloride from wastewater via Mikania micrantha Kunth-derived biochar modified by Zn/Fe-layered double hydroxide, *Bioresour. Technol.*, 2022, **361**, 127646.
64 L. Lonappan, T. Rouissi, R. K. Das, S. K. Brar, A. A. Ramirez, M. Verma, R. Y. Surampalli and J. R. Valero, Adsorption of methylene blue on biochar microparticles derived from different waste materials, *Waste Manage.*, 2016, **49**, 537–544.
65 J. Li, G. Yu, L. Pan, C. Li, F. You and Y. Wang, Ciprofloxacin adsorption by biochar derived from co-pyrolysis of sewage sludge and bamboo waste, *Environ. Sci. Pollut. Res. Int.*, 2020, **27**, 22806–22817.
66 H. Sun, Y. Lin, H. Takeshi, X. Wang, D. Wu and Y. Tian, Synthesis of 3D graphene-based materials and their applications for removing dyes and heavy metals, *Environ. Sci. Pollut. Res. Int.*, 2021, **28**, 52625–52650.
67 A. H. Jawad, A. S. Waheeb, R. Abd Rashid, W. I. Nawawi and E. Yousif, Equilibrium isotherms, kinetics, and thermodynamics studies of methylene blue adsorption on pomegranate (Punica granatum) peels as a natural low-cost biosorbent, *Desalin. Water Treat.*, 2018, **105**, 322–331.
68 H. Shao, Y. Li, L. Zheng, T. Chen and J. Liu, Removal of methylene blue by chemically modified defatted brown algae Laminaria japonica, *J. Taiwan Inst. Chem. Eng.*, 2017, **80**, 525–532.
69 B. Delley, Analytic energy derivatives in the numerical local-density-functional approach, *J. Chem. Phys.*, 1991, **94**, 7245–7250.
70 B. Delley, From molecules to solids with the DMol3 approach, *J. Chem. Phys.*, 2000, **113**, 7756–7764.
71 J. Hoslett, H. Ghazal, N. Mohamad and H. Jouhara, Removal of methylene blue from aqueous solutions by biochar prepared from the pyrolysis of mixed municipal discarded material, *Sci. Total Environ.*, 2020, **714**, 136832.

72 U. Habiba, S. Mutahir, M. A. Khan, M. Humayun, M. S. Refat and K. S. Munawar, Effective removal of refractory pollutants through cinnamic acid-modified wheat husk biochar: Experimental and DFT-based analysis, *Catalysts*, 2022, **12**, 1063.

73 S. Li, L. Huang, H. Zhang, Z. Huang, Q. Jia and S. Zhang, Adsorption mechanism of methylene blue on oxygen-containing functional groups modified graphitic carbon spheres: Experiment and DFT study, *Appl. Surf. Sci.*, 2021, **540**, 148386.

74 L. Sellaoui, D. Franco, H. Ghalla, J. Georgin, M. S. Netto, G. Luiz Dotto, A. Bonilla-Petriciolet, H. Belmabrouk and A. Bajahzar, Insights of the adsorption mechanism of methylene blue on brazilian berries seeds: Experiments, phenomenological modelling and DFT calculations, *Chem. Eng. J.*, 2020, **394**, 125011.

75 Y. An, X. Li, Z. Liu, Y. Li, Z. Zhou and X. Liu, Constant oxidation of atrazine in Fe(III)/PDS system by enhancing Fe(III)/Fe(II) cycle with quinones: Reaction mechanism, degradation pathway and DFT calculation, *Chemosphere*, 2023, **317**, 137883.

76 Z. Zhao, T. Nie and W. Zhou, Enhanced biochar stabilities and adsorption properties for tetracycline by synthesizing silica-composited biochar, *Environ. Pollut.*, 2019, **254**, 113015.

77 V. Nguyen, T. Nguyen, C. P. Huang, C. Chen, X. Bui and C. Dong, Alkaline modified biochar derived from spent coffee ground for removal of tetracycline from aqueous solutions, *J. Water Process Eng.*, 2021, **40**, 101908.

78 P. Zhou, X. Li, J. Zhou, Z. Peng, L. Shen and W. Li, Insights of the adsorption mechanism of methylene blue on biochar from phytoextraction residues of Citrus aurantium L.: Adsorption model and DFT calculations, *J. Environ. Chem. Eng.*, 2023, **11**, 110496.